HHS Public Access

Author manuscript

*Nucl Med Biol*. Author manuscript; available in PMC 2022 February 01.

Published in final edited form as:

*Nucl Med Biol*. 2021 February ; 93: 37–45. doi:10.1016/j.nucmedbio.2020.11.007.

# Synthesis and fluorine-18 radiolabeling of a phospholipid as a PET imaging agent for prostate cancer

**Kim H. Kwan**[a,*], **Ingrid J.G. Burvenich**[b,c,*], **Margaret M. Centenera**[d,e,*], **Yit Wooi Goh**[b], **Angela Rigopoulos**[b,c], **Jonas Dehairs**[f], **Johannes V. Swinnen**[f], **Ganesh V. Raj**[g], **Andrew J. Hoy**[h], **Lisa M. Butler**[d,e], **Andrew M. Scott**[b,c,i,j,**], **Jonathan M. White**[a,**], **Uwe Ackermann**[b,c,i,j,**]

[a]School of Chemistry, Bio21 Molecular Science and Biotechnology Institute, The University of Melbourne, Australia

[b]Tumour Targeting Laboratory, Olivia Newton-John Cancer Research Institute, Heidelberg, Australia

[c]School of Cancer Medicine, La Trobe University, Melbourne, Australia

[d]Adelaide Medical School and Freemasons Foundation Centre for Men's Health, University of Adelaide, Adelaide, Australia

[e]South Australian Health and Medical Research Institute, Adelaide, Australia

[f]Laboratory of Lipid Metabolism and Cancer, Department of Oncology, LKI - Leuven Cancer Institute, KU Leuven - University of Leuven, Leuven, Belgium

[g]Departments of Urology and Pharmacology, UT Southwestern Medical Center at Dallas, TX, USA

[h]School of Medical Sciences, The University of Sydney, Sydney

[i]Department of Molecular Imaging and Therapy, Austin Health, Heidelberg, Australia

[j]Department of Medicine, Melbourne University, Melbourne, Australia

## Abstract

**Introduction—**Altered lipid metabolism and subsequent changes in cellular lipid composition have been observed in prostate cancer cells, are associated with poor clinical outcome, and are promising targets for metabolic therapies. This study reports for the first time on the synthesis of a phospholipid radiotracer based on the phospholipid 1,2-didocosahexaenoyl-*sn*-glycero-3-

Address Corresponding authors: Uwe Ackermann, Department of Molecular Imaging and Therapy, Austin Health, Level 1 HSB, 145 Studley Road, Heidelberg, Melbourne 3084, Australia., uwea@unimelb.edu.au., Ingrid Burvenich, Tumour Targeting Laboratory, Olivia Newton-John Cancer Research Institute, Level 5, 145 Studley Road, Heidelberg, Melbourne 3084, Australia., Ingrid.burvenich@onjcri.org.au.

*,these authors contributed equally to this work

**,co-senior authors

phosphocholine (PC44:12) to allow tracking of polyunsaturated lipid tumor uptake via PET imaging. This tracer may aid in the development of strategies to modulate response to therapies targeting lipid metabolism in prostate cancer.

**Methods—**Lipidomics analysis of prostate tumor explants and LNCaP tumor cells were used to identify PC44:12 as a potential phospholipid candidate for radiotracer development. Synthesis of phosphocholine precursor and non-radioactive standard were optimised using click chemistry. The biodistribution of a fluorine-18 labeled analogue, N-{[4-(2-[$^{18}$F]fluoroethyl)-2,3,4-triazol-1-yl]methyl}-1,2-didocosahexaenoyl-*sn*-glycero-3-phosphocholine (**[$^{18}$F]2**) was determined in LNCaP prostate tumor-bearing NOD SCID gamma mice by *ex vivo* biodistribution and PET imaging studies and compared to biodistribution of [$^{18}$F]fluoromethylcholine.

**Results—**[$^{18}$F]**2** was produced with a decay-corrected yield of 17.8 ± 3.7 % and an average radiochemical purity of 97.00 ± 0.89% ($n$ = 6). Molar activity was 85.1 ± 3.45 GBq/μmol (2300 ± 93 mCi/μmol) and the total synthesis time was 2 hours. *Ex vivo* biodistribution data demonstrated high liver uptake (41.1 ± 9.2 %ID/g) and high splenic uptake (10.9 ± 9.1 %ID/g) 50 minutes post-injection. *Ex vivo* biodistribution showed low absolute tumor uptake of [$^{18}$F]**2** (0.8 ± 0.3 %ID/g). However, dynamic PET imaging demonstrated an increase over time of the relative tumor-to-muscle ratio with a peak of 2.8 ± 0.5 reached 1 hour post-injection. In contrast, dynamic PET of [$^{18}$F]fluoromethylcholine demonstrated no increase in tumor-to-muscle ratios due to an increase in both tumor and muscle over time. Absolute uptake of [$^{18}$F]fluoromethylcholine was higher and peaked at 60 minutes post injection (2.25 ± 0.29 %ID/g) compared to [$^{18}$F]**2** (1.44 ± 0.06 %ID/g) during the 1 hour dynamic scan period.

**Conclusions and advances in knowledge—**This study demonstrates the ability to radiolabel phospholipids and indicates the potential to monitor the *in vivo* distribution of phospholipids using fluorine-18 based PET.

### Keywords

Fluorine-18; phospholipid; lipid metabolism; PET; prostate cancer

## 1. Introduction

Currently, prostate cancer is the second most diagnosed cancer and the 5$^{th}$ leading cause of cancer-related mortality in men worldwide [1]. Prostate cancer is mainly driven by a growth response to androgens mediated by the androgen receptor (AR). Patients with metastatic disease receive androgen deprivation therapy, and although initially effective, relapse is expected to occur within 18–24 months for the majority of patients [2]. Castration-resistant prostate cancer patients demonstrate a variable response to the more effective FDA-approved agents targeting AR such as enzalutamide and abiraterone acetate [3]. Due to the variability in responses and duration of responses seen in patients, sensitive and selective imaging tools are needed in order to enable tumor localization and predicting response to therapy. Currently FDA approved positron emission tomography (PET) imaging agents for prostate cancer include metabolic imaging agents [$^{11}$C]-choline and [$^{18}$F]fluorocholine for PET [4]. Imaging agents targeting prostate-specific membrane antigen (PSMA) have gained importance in the diagnosis and treatment of prostate cancer [4–7].

Altered lipid metabolism is a hallmark feature of most cancers including prostate cancer [8]. These alterations are geared towards the support of membrane and bioactive liquid synthesis required for growth and proliferation. They support energy supply, and altered cellular lipid profiles facilitate signaling and survival, and protect cells from stress and insults. Prostate cancer cells tend to be highly lipogenic, but can also take up lipids from the microenvironment [9–11]. The relative contribution between fatty acid synthesis and uptake changes the balance between polyunsaturated fatty acids (PUFA) and mono-unsaturated fatty acids (MUFA). In addition, PUFAs have shown to improve response to therapy as well as determine tumor progression, apoptosis and differentiation [11–13]. PUFA can be taken up as free fatty acid from diet but also as intact phospholipids [11]. Active research is currently being done on ways to increase PUFA content through enzyme and pathway modulation as well as via dietary intake [10–12, 14–16].

A range of approaches have been used to study altered lipid profiles in prostate cancer [8, 13]. Monitoring changes in the lipid metabolism based on *de novo* synthesis has been investigated via [$^{11}$C]-choline and [$^{18}$F]fluorocholine, [$^{11}$C]-acetate and other fatty acids labeled with carbon-11 and fluorine-18 [17]. However, these metabolic imaging agents often are incorporated in different metabolic pathways and cannot track changes in specific phospholipid species within the bilayer cellular membrane in response to androgen regulation. In this study, we show that PC44:12 is a highly androgen regulated polyunsaturated phospholipid in prostate cancer. Radiolabeling of PC44:12 phospholipid with a positron emitting radionuclide will allow us to follow the uptake of polyunsaturated lipids and may aid in the development of strategies to monitor and modulate response to androgen receptor targeted therapies.

This publication reports on the synthesis of a phospholipid radiotracer based on the phospholipid 1,2-didocosahexaenoyl-*sn*-glycero-3-phosphocholine (PC44:12) **(1)** (Fig. 1): [$^{18}$F]**2**. Due to our extensive experience with 2-[$^{18}$F]fluoroethyl azide click chemistry as well as the compatibility of this strategy with a large number of functional groups, we chose a click chemistry approach to radiolabel the PC44:12 phospholipid at the N-methyl position [18, 19]. To demonstrate its possible use as a radiotracer for prostate cancer, initial biodistribution and tumor uptake in LNCaP tumor-bearing mice was evaluated and compared to [$^{18}$F]fluoromethylcholine via dynamic PET imaging.

## 2. Materials and methods

### 2.1. General

Solvents and reagents were purchased from Sigma-Aldrich. 2-Azidoethyl 4-toluenesulfonate and 2-fluoroethyl 4-toluenesulfonate were synthesised using published procedures [20, 21]. Purification by silica gel chromatography was performed using a Biotage Isolera automated flash chromatography instrument and Reveleris cartridges (4 g, 12 g). NMR spectra were recorded on either a Varian INOVA 400 or 600 instrument, with operating frequencies of 400 MHz for $^{1}$H NMR and 100 MHz for $^{13}$C NMR. High resolution electrospray ionisation (ESI) mass spectrometry (MS) was conducted using a Thermo Scientific Exactive Plus Orbitrap mass spectrometer. Liquid chromatography (LC)-MS was conducted with an Agilent 6200 Series Accurate-Mass Time-Of-Flight instrument and Agilent Eclipse XDB-

C18 5 μm 4.6 × 150 mm column. Radiotracer and radioactive metabolite analysis were run on a Shimadzu Prominence LC-20AT system with a SPD-20A UV/Vis detector and radioactivity detector using a Phenomenex Luna 5 μm 150 × 4.6 mm C18 column.

Collision induced dissociation mass spectrometry was conducted on a Thermo Finnigan LTQ ESI mass spectrometer. Samples were prepared in 100 μM methanol and injected into the ESI source at a 5 μL $min^{-1}$ flow rate. The instrument was tuned to optimise the signal of the desired parent ion peak. The ESI source conditions were maintained at the following parameters: 2.5–4.7 kV needle potential, 250°C capillary temperature, 0.0–34.0 V capillary voltage, and 0.0–55.0 V tube lens voltage. An ion gauge pressure of $0.69 \times 10^{-5}$ torr was maintained using helium. Ions of interest for $MS^n$ experiments were isolated with a 1–4 *m/z* window and 25 – 30 eV collision energy was applied for dissociation.

[$^{18}$F]fluoride was produced using an IBA Cyclone 10/5 cyclotron at the Centre of Positron Emission Tomography, Austin Hospital. Irradiation of [$^{18}$O]$H_2O$ using a 10 MeV proton beam in a titanium target induces a $^{18}O(p,n)^{18}F$ reaction and a beam current of 22 uA over 30 minutes generated 11.1–18.5 GBq (300–500 mCi) of [$^{18}$F]fluoride.

Synthesis of the phospholipid radiotracer was performed using the automated FlexLab module by iPhase Technologies.

[$^{18}$F]fluoromethylcholine was obtained from the Department of Molecular Imaging and Therapy (Austin Hospital) and was synthesised on a GE Tracerlab MX module using reagents and methods commercially available from ABX, Radeberg, Germany.

### 2.2. ESI-MS/MS-based lipidomics of androgen and/or anti-androgen treated LNCaP cells and patient-derived prostate tumor explants (PDEs)

**Cell line:** Human prostate cancer cell line LNCaP was obtained from American Type Culture collection and grown in RPMI 1640 medium (Life technologies) supplemented with 10% fetal bovine serum (FBS) and 2 mM L-Glutamine (Life technologies). For androgen treatment, cells were seeded in 100 mm dishes in culture medium supplemented with 5% dextran charcoal coated FBS for 24 hours prior to addition of 1 nM mibolerone. For anti-androgen treatment, cells were seeded 100 mm dishes in culture medium supplemented with 10% FBS for 24 hours prior to treatment with 1 μM enzalutamide (ENZ). Cells were cultured for 72 hours, until they reached 70–90% confluency, were washed with PBS and collected in 800 μL PBS by scraping. Lipids were extracted from cells and subjected to lipidomics as described below.

**PDEs:** Deidentified fresh prostate cancer tissues were obtained with written informed consent from men undergoing radical prostatectomy for high volume cancer at the Hospitals of the University of Texas Southwestern Medical Center (Dallas, TX, USA). Protocols were approved by the University's Institutional Review Board and research conducted according to the standards set by the Declaration of Helsinki. Tissues were dissected into explants and cultured as described previously [22], in the presence of vehicle (DMSO), 10 μM bicalutamide, or 10 μM ENZ. PDEs were cultured at 37°C for 48h, then half was formalin-fixed and paraffin embedded for immunohistochemistry evaluation of the proliferative

marker Ki67 as described previously [22] and half was snap frozen and stored at −80°C for lipidomics. PDEs were prepared for lipidome analysis by homogenizing in 500 μL ice cold PBS using the Precellys tissue homogenizer (Bertin Technologies, Montigny-le-Bretonneux, France). Samples were transferred to an Eppendorf tube and topped up to 800 μL PBS prior to lipid extraction and lipidomics as described below.

**Lipidomics:** PDEs and cells were prepared in 800 μL PBS as described above. An aliquot of 100 μL was set to quantify DNA for normalization. Lipids were extracted from the remaining 700 μL using a modified Bligh-Dyer protocol by adding 800 μL $CHCl_3$, 900 μL 1N HCl:$CH_3OH$ 1:8 (v/v) and 500 μg of the anti-oxidant 2,6-di-tert-butyl-4-methylphenol (Sigma). Following centrifugal phase separation, the lower organic fraction was collected, evaporated, and the lipid pellet stored under argon gas at −20 °C. Lipid pellets were reconstituted in diluent ($CH_3OH$:$CHCl_3$:$NH_4OH$; 90:10:1.25, v/v/v) according to DNA quantification (1 μL diluent / 1 μg DNA). Phospholipid species were analyzed by ESI-MS/MS on a hybrid quadrupole linear ion trap mass spectrometer (4000 QTRAP system; Applied Biosystems, Foster City, CA) equipped with a TriVersa robotic nanosource (Advion Biosciences) as described previously [23].

### 2.3. Precursor and non-radioactive standard synthesis

N-desmethyl- L-α-glycerophosphorylcholine **(3)** (Fig. 2): L-α-glycerophosphorylcholine (GPC) (60 mg, 0.233 mmol) and 1,4-diazabicyclo[2.2.2]octane (DABCO) (158 mg, 1.41 mmol) in dry dimethylformamide (DMF) (1.5 ml) were stirred and heated to 150°C in a dry sealed tube under nitrogen for 7 h [24]. Solvent was removed via nitrogen stream to give the crude product as a brown oil which was used in the next step without further purification (85%).

Calculated *m/z*: 244.0945 *m/z* $[M+2H]^+$, 242.0872 *m/z* $[M]^-$

Measured ESI-MS: 244.09 *m/z* $[M+2H]^+$, 242.0792 *m/z* $[M]^-$

N-desmethyl-1,2-didocosahexaenoyl-*sn*-glycero-3-phosphocholine **(4):** cis-4,7,10,13,16,19-docosahexaenoic acid (DHA) (190 μL, 180 mg, 0.545 mmol), 2,4,6-trichlorobenzoyl chloride (124 μL, 194 mg, 0.794 mmol), 4-dimethylaminopyridine (DMAP) (242 mg), and dry triethylamine (TEA) (207 μL, 151 mg, 1.488 mmol) in dry DMF (1 mL) were mixed under nitrogen and in darkness. **(3)** (0.233 mmol) was added and stirred at room temperature for 20 h. Dry diethyl ether was added and the precipitate was filtered off. Solvent was removed from the filtrate in-vacuo and via nitrogen stream. Silica column chromatography was conducted using a 0 – 100% methanol in dichloromethane (DCM) with a 0.1% triethylamine solvent system. Detection was via a UV detector at 206 nm and manual ESI-MS with product elution at 10 – 20% methanol in DCM. Fractions were combined with 2 mg butylated hydroxytoluene (BHT) added and solvent removed in-vacuo. Dry THF was added to the product and cooled to 0°C. The triethylamine hydrochloride salt was filtered off, and Dowex – X8 Na form ion exchange resin beads were added to the filtrate and allowed to stand for 1 h. The beads were removed and solvent removed under nitrogen stream to give product as a yellow oil (166 mg, 0.196 mmol, 83%).

Calculated *m/z*: 864.5538 *m/z* $[M+2H]^+$, 862.5392 *m/z* $[M]^-$

Measured ESI-MS: 864.5543 *m/z* $[M+2H]^+$, 862.5018 *m/z* $[M]^-$

Measured CID-$MS^n$ (+): $MS^2$ 695.3 *m/z*, $MS^3$ 385.3 *m/z*

$^1$H NMR (400 MHz, CDCl3) δ 5.46 – 5.19 (m, 25H), 4.48 – 4.33 (m, 1H), 4.26 (t, *J* = 9.8 Hz, 2H), 4.17 (dd, *J* = 12.0, 6.6 Hz, 1H), 4.08 – 3.95 (m, 2H), 3.20 (s, 2H), 2.93 – 2.70 (m, 26H), 2.44 – 2.30 (m, 8H), 2.07 (p, *J* = 7.3 Hz, 4H), 0.97 (t, *J* = 7.5 Hz, 6H).

$^{13}$C NMR (600 MHz, CDCl3): 8.88, 14.40, 22.72, 25.66, 25.72, 25.75, 30.44, 34.03, 34.21, 44.49, 45.76, 58.69, 58.76, 60.83, 60.88, 62.91, 63.74, 63.79, 70.67, 125.62, 127.91, 127.98, 128.14, 128.18, 128.35, 129.39, 128.42, 128.68, 129.45, 132.14, 151.62, 172.47, 172.82

N-propargyl-1,2-didocosahexaenoyl-*sn*-glycero-3-phosphocholine **(5):** Propargyl bromide in toluene (150 μL) was added to sodium iodide (100 mg) in dry acetonitrile (1 mL) and stirred for 5 min at RT. After the sodium bromide precipitate settled, the remaining yellow propargyl iodide solution was transferred to **(4)** (30 mg, 0.035 mmol) with dry TEA (50 μL) under nitrogen and stirred at room temperature for 24 h. The salt was filtered off and the solvent removed from the filtrate by nitrogen stream. Silica column chromatography (0 – 100% methanol in DCM with 0.1% triethylamine) gave product at 50% methanol. BHT was added and solvent was removed in-vacuo. Dry THF was added and cooled to 0°C for 2 h. Salt precipitate was filtered off and Dowex X-8 Na form ion exchange resin beads were added and left for 2 h at room temperature. This was filtered and solvent removed by nitrogen stream to give a yellow oil (25 mg, 0.028 mmol, 80%).

Calculated *m/z*: 902.5695 *m/z* $[M+H]^+$

Measured ESI-MS: 902.5720 *m/z* $[M+H]^+$

$^1$H NMR (600 MHz, CDCl3) δ 5.44 – 5.27 (m, 24H), 5.22 (td, *J* = 8.9, 5.7 Hz, 1H), 4.65 (s, 2H), 4.39 (dt, *J* = 17.0, 8.5 Hz, 1H), 4.34 (s, 2H), 4.15 (dd, *J* = 12.0, 6.9 Hz, 1H), 4.03 – 3.92 (m, 2H), 3.89 (s, 2H), 3.42 (s, 6H), 2.92 – 2.75 (m, 20H), 2.47 – 2.31 (m, 9H), 2.10 – 1.99 (m, 4H), 0.96 (t, *J* = 7.5 Hz, 6H).

$^{13}$C NMR (600 MHz, CDCl3): 14.24, 20.53, 22.25, 25.51, 25.57, 25.60, 33.90, 34.09, 51.85, 55.33, 59.03, 62.97, 63.42, 63.46, 64.49, 70.69, 70.73, 71.67, 81.22, 126.97, 127.77, 127.82, 127.98, 128.02, 128.26, 128.31, 128.32, 128.55, 129.30, 132.01, 172.46, 172.78

N-{[4-(2-fluoroethyl)-2,3,4-triazol-1-yl]methyl}-1,2-didocosahexaenoyl-*sn*-glycero-3-phosphocholine **(2):** Fluoroethyl tosylate and sodium azide were mixed in dry DMF at room temperature for 24 h to give fluoroethyl azide. Crude product was used for the next step without further purification. Copper (I) iodide (2.5 mg) and sodium ascorbate (26 mg) were dissolved in water (250 μL) before addition of acetonitrile (250 μL), DMF (200 μL) and DIPEA (25 μL). This was mixed vigorously until the mixture became orange. This catalyst mixture was added to **(5)** (7.7 mg, 0.0085 mmol) with crude fluoroethyl azide and stirred for 24 h. Solvent was removed via nitrogen stream with gentle heating. Silica column chromatography was conducted using a 0 – 100% methanol in DCM with a 0.1%

triethylamine solvent system. Product eluted at 60% methanol in DCM as detected with 206nm UV detection and manual ESI-MS. Solvent was removed in-vacuo. Dry THF was added and cooled to 0°C. Salt precipitate was filtered off and Dowex X-8 Na form ion exchange resin beads were added and left for 2 h at room temperature. This was filtered and solvent removed by nitrogen stream to give a yellow oil (7.6 mg, 0.0077 mmol, 95%).

Calculated *m/z*: 991.6011 *m/z* $[M+H]^+$

Measured ESI-MS: 991.6088 *m/z* $[M+H]^+$

Measured CID-$MS^n$ (+): $MS^2$ 695.3 *m/z*, $MS^3$ 385.3 *m/z*

$^1$H NMR (600 MHz, CDCl3) δ 8.75 (s, 1H), 5.54 – 5.17 (m, 24H), 5.22 (d, J = 3.2 Hz, 1H), 4.98 – 4.67 (m, 6H), 4.46 – 4.30 (m, 3H), 4.22 – 4.05 (m, 1H), 3.97 (d, J = 4.8 Hz, 2H), 3.65 (d, J = 20.9 Hz, 2H), 3.28 (s, 6H), 2.94 – 2.69 (m, 20H), 2.40 – 2.29 (m, 8H), 2.06 (p, J = 7.4 Hz, 4H), 0.95 (t, J = 7.5 Hz, 6H).

$^{13}$C NMR (600 MHz, CDCl3): 8.57, 14.24, 20.52, 22.52, 22.54, 25.50, 25.55, 25.59, 29.50, 29.65, 33.86, 34.03, 45.70, 50.65, 50.79, 59.18, 59.62, 62.79, 63.61, 64.24, 70.53, 80.51, 81.65, 126.96, 127.70, 127.73, 127.81, 127.95, 128.01, 128.0, 128.25, 128.30, 128.32, 128.53, 129.32, 129.82, 131.99, 135.74, 172.43, 172.74.

### 2.4. N-{[4-(2-[$^{18}$F]fluoroethyl)-2,3,4-triazol-1-yl]methyl}-1,2-didocosahexaenoyl-*sn*-glycero-3-phosphocholine ([$^{18}$F]**2**)

Isolation of the F-18 fluoride ion from $[^{18}O]H_2O$ was achieved by trapping on a Chromafix PS-$HCO_3$ ion exchange column. The column was eluted with a solution containing $KHCO_3$ (2 mg) and kryptofix 2.2.2 (11 mg) in a mixture of 1 mL of methanol and 200 μL of water. Evaporation to dryness with 1 mL of acetonitrile gave the anhydrous [$^{18}$F]fluoride used in the labeling experiments.

The dried [$^{18}$F]KF/Kryptofix complex was reacted with azidoethyltosylate (4 μL) in dry acetonitrile (750 μL) at 90°C over 7 min to give 2-[$^{18}$F]fluoroethyl azide. 2-[$^{18}$F]fluoroethyl azide was distilled at 100°C into a second reactor according to published procedure [18]. Precursor **(5)** (2.5 – 3.3 mg) in DMF was added to the 2-[$^{18}$F]fluoroethyl azide. Catalyst (prepared separately by dissolving copper (I) iodide (2.5 mg) and sodium ascorbate (26 mg) in water (250 μL) before addition of acetonitrile (250 μL), DMF (200 μL) and DIPEA (25 μL) and mixed vigorously until it turned orange) was added and stirred at 70°C for 20 minutes. Mixture was diluted with water (11 mL) and product was trapped on a C18 Sep-Pak and washed with water (10 mL). Radiotracer was eluted with ethanol (1.5 mL) and dried under argon stream with gentle heating in a warm water bath. This was reformulated into a maximum 10% ethanol in water solution. For quality control, formulated radiotracer was injected into an HPLC with a gradient of 5 – 95% ethanol in water over 10 minutes followed by 20 minutes of 95% ethanol at a flow rate of 0.5 mL per min. Stability was tested by a subsequent injection of formulated radiotracer into the HPLC after 7 hours at room temperature.

### 2.5. Estimation of lipophilicity

Traditional octanol/phosphate buffer method: 5 μL of [$^{18}$F]**2** was added to 500 μL octanol and 500 μL of phosphate buffer adjusted to pH 7.4. After vortexing for 3 minutes, the sample was centrifuged at 12,000 rpm for 5 minutes. 100 μL was carefully taken out of each phase and the radioactivity measured.

Chromatographic hydrophobicity index approach: on an Agilent C18 4.6 × 150 mm column, **2** and reference compounds were injected individually and run using a gradient of 0 – 100% methanol in water over 20 minutes followed by 35 minutes 100% methanol at a flow rate of 0.3 mL/min. The reference compounds included choline, caffeine, ibuprofen, trans-retinoic acid, cholecalciferol, and α-tocopherol. Reference calculated log *P* values were sourced from online tools ALOGPS 2.1 [25] and ChemAxon (MarvinSketch, 2018).

### 2.6. Stability studies

17 μL human serum in 33 μL phosphate buffer was incubated at 37°C with 2.5 μL formulated [$^{18}$F]**2**. At the 1 and 2 hour time points, 15 μL methanol was added and centrifuged for 5 minutes. The supernatant was carefully taken out and radioactivity of both supernatant and the remaining pellet was counted.

### 2.7. Animal Experiments

Animal experiments were approved by the Austin Health animal ethics committee and performed according to the NHMRC Australian code of practice for the care and use of animals for scientific purposes.

LNCaP cells ($5 \times 10^6$ cells in 50 μL RPMI 1640 culture medium (Invitrogen) and 50 μL Matrigel (BD)) were injected subcutaneously in 6-week-old NOD SCID gamma male mice. Tumors were measured using a calliper and upon reaching approximately 200 mm$^3$, mice were used for PET/MR imaging.

### 2.8. PET/MR Imaging and biodistribution

Mice were injected with 14.8 MBq (0.4 mCi) of [$^{18}$F]**2** or [$^{18}$F]fluoromethylcholine via the lateral tail veins. Under isoflurane anaesthesia, mice were imaged using a multimodality positron emission tomography (PET) and magnetic resonance (MR) camera (nanoScan®, Mediso, Budapest, Hungary). The mice were anesthetized with isoflurane during PET/MR imaging. Dynamic scans (60 minutes, 10 minutes per frame) were performed immediately after injection of [$^{18}$F]**2** ($n = 2$) or [$^{18}$F]fluoromethylcholine ($n = 2$) followed by a 25-minute MR scan. PMOD software was used for co-registration and mark-up of volumes of interest (VOI) in cross-sectional MR images. Standard uptake values (SUVs) were generated by measuring VOI from PET/MR images. SUV values were calculated with the formula: SUV = $C_{PET}(T)$(kBq/mL) / [ID (kBq)/ BW (g)] with $C_{PET}(T)$ = radioactivity concentration in tissue of interest at time $T$; ID, injected dose and BW, body weight. To convert (kBq/cc)/ccm to %ID/ccm, total body uptake (kBq/cc) of each mouse was used as an approximation of ID. For biodistribution, a separate group of mice ($n = 3$) were injected intravenously with 14.8 MBq (0.4 mCi) [$^{18}$F]**2** and at 50 minutes post injection, mice were sacrificed and selected organs were removed, and counted in a gamma counter (Perkin Elmer Wizerd2). To

calculate injected dose and correct for radioactive decay, standards (20-fold dilution of injected dose) were prepared in triplicate and counted for radioactivity at the same time of the tissue samples.

### 2.9. Metabolism studies

After imaging was completed, liver and blood were harvested from mice injected with [$^{18}$F]**2** used in the dynamic PET/MR study. Liver tissue was homogenised in 2:1 chloroform/methanol before being filtered off. The filtrate was centrifuged for 5 minutes, and the organic and aqueous layers injected into the HPLC. Blood extracts were centrifuged at 2000 g for 5 minutes. 50 μL of the supernatant was combined with 50 μL methanol and centrifuged for 5 minutes. 40 μL of water was added to the supernatant and then injected into the HPLC. All HPLC injections were run with a gradient of 5 – 95% ethanol in water over 10 minutes followed by 20 minutes of 95% ethanol at a flow rate of 0.5 mL/min.

### 2.10. Statistical analysis

Data are presented as mean ± standard error. Two-tailed unpaired t-test was performed using Graphpad Prism 5.04.

## 3. Results and discussion

### 3.1. PC44: 12, a highly polyunsaturated phospholipid regulated by androgen in prostate cancer

To identify a suitable candidate phospholipid for probe development, androgen regulated changes in phosphatidylcholine (PC) lipid abundance were measured via lipidomics analysis in prostate cancer cell lines and patient-derived prostate tumors (data not shown). The main selection criterion for a suitable candidate for probe development was the display of altered abundance of the phospholipid species in response to androgen regulating reagents (i.e. synthetic androgen mibolerone (MIB) and androgen receptor (AR) antagonist enzalutamide (ENZ)). Additionally, an increase in abundance of a phospholipid candidate for probe development was preferred as this would allow the measurement of an increase in PET signal in responding tumours in response to androgen receptor targeted therapies in prostate cancer patients. Although multiple phospholipid species matched these criteria (data not shown), PC44:12 was selected as an example phospholipid for initial work up of the radiolabeling conditions for fluorine-18 radiolabeling of phospholipids.

Lipidomic analysis of prostate cancer cell line LNCaP showed a significant decrease in the abundance of phospholipid species PC44:12 in the presence of synthetic androgen MIB compared to vehicle treated cells, and a significant increase in the presence of AR antagonist ENZ (Fig. 3A). As a more clinically-relevant model system, patient derived prostate tumour explants cultured in the presence of AR antagonists bicalutamide (10 μM) or ENZ (10 μM) were also subjected to lipidomics analysis. Prior to evaluating lipid changes, PDEs were categorised into two categories based on their proliferative response to AR antagonism, where non-responders were defined as having <50% change in the proliferative marker Ki67 compared to matched vehicle treated PDEs, and responders >50% change in Ki67 positivity (Fig. 3B). A significant increase in the PUFA species PC44:12 was observed in responders

to AR antagonism compared to non-responders (Fig 3C). Based on its significant stimulation upon AR targeting in prostate cancer cells and patient-derived tumors, PC44:12 was selected as an initial candidate for radiotracer development.

### 3.2. Synthesis of phosphatidylcholine precursor and non-radioactive standard

Synthesis of precursor and non-radioactive standard necessitated an inert atmosphere to limit air autoxidation (Fig. 2). After coupling of two DHA to demethylated GPC, **(4)** was reacted with propargyl iodide to give the alkyne precursor **(5)** with a yield of 80%. The propargyl derivative **(5)** was then reacted with 2-fluoroethyl azide in a copper(I) catalysed azide-alkyne cycloaddition reaction to give the non-radioactive standard **2** with a yield of 95%.

### 3.3. Radiolabeling of [$^{18}$F]2

We chose to employ 2-[$^{18}$F]fluoroethyl azide click chemistry as our radiolabeling strategy since this method is easy to automate, is compatible with the functional groups present in the phospholipid precursor and produces radiopharmaceuticals in high yields and good molar activity. Distillation of 2-[$^{18}$F]fluoroethyl azide was performed at 100°C. A copper iodide/ sodium ascorbate catalyst was used to promote the click reaction between 2-[$^{18}$F]fluoroethyl azide and the precursor alkyne **(5)**.

Preparative C18 HPLC failed to reproducibly separate product from by-products despite attempts with acetonitrile, ethanol or ammonium acetate additives. For [$^{18}$F]fluoromethylcholine, cation exchange cartridges such as CM Light Sep-pak cartridges are routinely used to purify the radiotracer. In the case of [$^{18}$F]**2**, solid phase extraction using a C18 Sep-Pak was sufficient for removal of radioactive side products and unreacted precursor. This method was also found to be superior to traditional HPLC purification. Purification was conducted by dilution of reaction products with water (11 mL) and trapping the radiotracer on a C18 Sep-Pak, followed by an aqueous wash (10 mL) which successfully removed the reagents and polar radioactive side products to give radiochemically and chemically pure product. Elution with ethanol (1.5 mL) and drying under argon gave the [$^{18}$F]**2** which was reformulated into a maximum 10% ethanol in water solution.

[$^{18}$F]**2** was produced with a decay-corrected yield of 17.8 ± 3.7 % and an average radiochemical purity of 97.00 ± 0.89% ($n$ = 6, Table 1). Molar activity was 85.1 ± 3.45 GBq/ μmol (2300 ± 93 mCi/ μmol) and the total synthesis time was 2 h. Quality control analysis using HPLC demonstrated elution of non-radioactive standard and radiotracer at 24 minutes (Fig. 4). After 7 hours at room temperature, the final formulation showed no defluorination or degradation.

### 3.4. Estimation of lipophilicity

The traditional octanol/phosphate buffer method was initially attempted, but due to the highly hydrophobic nature of lipids, quantitation of lipid concentration in the aqueous phase was inaccurate. Hence, the chromatographic hydrophobicity index approach was taken in which the retention time of a molecule on a reverse phase system was correlated to its log $P$ [26]. A simplified version was conducted here where for a given chromatographic method, retention times of the non-radioactive standard **2** was compared with retention times of

reference compounds with calculated log *P* values [27]. Linear relationships between retention time and log *P* were established [ALOGPS: y = 0.2723x – 4.2669; $R^2$ = 0.9675; ChemAxon: y = 0.3063x – 5.4062; $R^2$ = 0.9723] and from this, the log *P* of **2** was approximated to be between 6.9 and 7.2 (Table 2). The high log *P* value reflects the expectation of the lipid tracer to passively cross cell membranes.

### 3.5. PET/MR imaging and biodistribution of [$^{18}$F]2 in LNCaP tumor-bearing mice

To evaluate [$^{18}$F]**2** as a potential imaging agent for prostate cancer, PET/MR imaging and biodistribution studies of [$^{18}$F]**2** were performed in LNCaP tumor-bearing NOD SCID gamma mice and compared to tumor uptake and biodistribution of [$^{18}$F]fluoromethylcholine. Figure 5 shows a representative whole-body maximum intensity projection (MIP) image at 60 minutes post injection for [$^{18}$F]**2** (Fig. 5A) and [$^{18}$F]fluoromethylcholine (Fig. 5D). Quantitative analysis of dynamic PET images showed high uptake in liver starting at 20.5 ± 2.5 %ID/cc at 10 minutes post injection, reaching 27.3 ± 3.1 %ID/cc at 60 minutes post injection for [$^{18}$F]-PC44:12. Bladder also showed increase in activity over time, increasing from 4.5 ± 1.0 %ID/cc at 10 minutes post injection to 24.5 ± 4.4 %ID/cc at 60 minutes post injection. In contrast, heart, lungs, kidneys and muscle had reached peak activity by 10 minutes post injection. Kupffer cells are known to take up free phospholipids, and this was reflected in the rapid and high liver uptake seen with [$^{18}$F]**2** [28]. [$^{18}$F]fluoromethylcholine showed an initial liver uptake of 13.7 ± 0.1 %ID/cc at 10 minutes post injection which reached 14.5 ± 1.2 %ID/cc at 60 minutes post injection. [$^{18}$F]**2** uptake in bladder was more prominent than [$^{18}$F]fluoromethylcholine, suggesting a higher renal excretion of [$^{18}$F]**2** compared to [$^{18}$F]fluoromethylcholine. Accumulation of [$^{18}$F]**2** in the bladder increased from 4.5 ± 1.0 %ID/cc to 24.5 ± 4.4 %ID/cc at 60 minutes post injection compared to low bladder uptake seen with [$^{18}$F]fluoromethylcholine (2.8 ± 1.2 %ID/cc at 10 minutes post injection versus 3.0 ± 0.6 %ID/cc at 60 minutes post injection).

Tumor uptake of [$^{18}$F]**2** was low (Fig. 5C). However, [$^{18}$F]**2** uptake in the tumor was retained over time (1.3 ± 0.3 %ID/cc at 10 minutes versus 1.4 ± 0.1 %ID/cc at 60 minutes after injection), whilst the muscle concentration decreased over time (1.1 ± 0.2 %ID/cc at 10 minutes versus 0.6 ± 0.1 %ID/cc at 60 minutes after injection). This resulted in an increase in tumor-to-muscle ratio from 1.2 ± 0.3 at 10 minutes post injection to 2.4 ± 0.2 at 60 minutes post injection. In contrast, for [$^{18}$F]fluoromethylcholine, both tumor and muscle retained [$^{18}$F]fluoromethylcholine over time (Fig. 5F). Therefore, the tumor-to-muscle ratio for [$^{18}$F]fluoromethylcholine did not show increase over time (0.90 ± 0.01 at 10 minutes post injection to 1.0 ± 0.1 at 60 minutes post injection).

In a final experiment, LNCaP tumor-bearing mice were injected with [$^{18}$F]**2**, followed by biodistribution at 50 minutes post injection (Table 3). Biodistribution data confirmed high liver uptake (41.1 ± 9.2 %ID/g), but lower activity in heart (2.39 ± 9.2 %ID/g) and lungs (3.48 ± 1.15 %ID/g) compared to imaging data (Table 3). In general, data obtained from the biodistribution study confirmed tissue distribution obtained from dynamic PET quantitation, although some differences in absolute uptake values between PET and biodistribution data observed might reflect the contribution of blood volume and blood activity contributing to each organ at time point of imaging. Some difference between organs weights (g) and organs

volumes (cc) may also contribute to differences seen between PET and biodistribution measurements. Although absolute values determined with biodistribution were lower for muscle (0.3 ± 0.1 %ID/g) and tumor (0.8 ± 0.3 %ID/g) compared to quantitative PET analysis, the relative tumor-to-muscle ratio determined via biodistribution (2.8 ± 0.5) was similar to the tumor-to-muscle ratio determined with quantitative PET analysis (2.4 ± 0.2). While this offers better differentiation and contrast between tumor and background for [$^{18}$F]**2** compared to [$^{18}$F]fluoromethylcholine, the overall low tumor uptake may limit the utility of [$^{18}$F]**2** for imaging of prostate cancer in the clinic.

The initial evaluation of phospholipid changes in LNCaP cells and patient derived explants, were determined as fold-change and therefore did not reflect the absolute amounts of each phospholipid species measured. Because of the low tumour uptake measured with [$^{18}$F]**2**, LNCaP tumors used in biodistribution studies were analysed via ESI-MS/MS-based lipidomics to determine prevalence of PC44:12. Of all phosphatidylcholine species measured, PC44:12 species only represented 0.02% of total PC species (3 nmol lipid per mg of DNA). In contrast, more abundant species (e.g. PC32:0, PC34:1, PC36:1, PC34:2, PC36:4) had a prevalence between 5 to 25%, 250 to 2500-fold higher compared to PC44:12. The low absolute amount of PC44:12 in LNCaP tumour cells might explain the low uptake of [$^{18}$F]**2** by LNCaP *in vivo*.

### 3.6. Metabolism studies

To determine the metabolic fate of [$^{18}$F]**2**, metabolites were analysed in plasma and liver extracts obtained from the biodistribution study. A minor polar metabolite was observed at 4 minutes into the HPLC run of the aqueous liver extract (Fig. 6). Given the early elution time and absence of this metabolite in the organic phase, it is likely cleavage of the polar headgroup. The metabolite accounted for 4 – 9.5% of total radioactivity after the two-hour process of imaging, biodistribution and organ harvest ($n$ = 2). Figure 7 shows the [$^{18}$F]**2** stability in blood, with 27% bound to plasma protein at 2 hours, and the remainder unbound. The metabolism assays indicate that the radiotracer was stable in blood and able to reach its target tissue intact.

## 4. Conclusions

This study demonstrates for the first time the ability to radiolabel phospholipids with fluorine-18 to high radiochemical purity. The [$^{18}$F]**2** phospholipid probe demonstrated low absolute uptake in tumors of LNCaP-tumor-bearing mice, but retained its integrity *in vivo* and demonstrated an increase in tumour-to-muscle ratio between 10 to 60 minutes, suggesting some [$^{18}$F]**2** phospholipid is retained within the tumour. Further research in mice is warranted to evaluate if fluorine-18 labeled phospholipids can distinguish between androgen-dependent and androgen-independent tumors, or can predict response to androgen deprivation therapies.

## Acknowledgements

We acknowledge the Australian Cancer Research Foundation for providing funds to purchase the nanoPET/MRI and nanoSPECT/CT imaging equipment. We utilized the services of the Simmons Cancer Center's Tissue Management Shared Resource at UT Southwestern Medical Center at Dallas. Research reported in this publication

was supported by the National Cancer Institute of the National Institutes of Health under award number P30 CA142543. This research was also undertaken using the Solid Target Laboratory, an ANSTO-Austin-LICR Partnership and with the support of the Operational Infrastructure Support Program of the Victorian State Government. We also acknowledge the use of the Melbourne Mass Spectrometry and Proteomics Facility (MMSPF) of the Bio21 Molecular Science and Biotechnology Institute at The University of Melbourne for the support of mass spectrometry analysis. AJH is supported by a Robinson Fellowship and funding from the University of Sydney. JVS is supported by the Research Foundation – Flanders (FWO G.0841.15 to JVS), the Stichting tegen Kanker (to JVS), KU Leuven (C16/15/073 and C32/17/052 to JVS), Interreg V-A (EMR23 “EURLIPIDS”). LMB was supported by an Australian Research Council Future Fellowship (130101004), and a Beat Cancer SA Beat Cancer Project Principal Cancer Research Fellowship (PRF1117). AMS was supported by an NHRMC Senior Investigator grant (477837). LMB, JVS, AS, and AJH are supported by the Movember Foundation and the Prostate Cancer Foundation of Australia (MRTA3). GVR is supported by the Prostate Cancer Foundation and the Department of Defense.

## References

[1]. Bray F, Ferlay J, Soerjomataram I, Siegel RL, Torre LA, and Jemal A. Global cancer statistics 2018: GLOBOCAN estimates of incidence and mortality worldwide for 36 cancers in 185 countries. Ca-Cancer J Clin 2018;68:394–424. [PubMed: 30207593]

[2]. Asmane I, Ceraline J, Duclos B, Rob L, Litique V, Barthelemy P, et al. New Strategies for Medical Management of Castration-Resistant Prostate Cancer. Oncology-Basel 2011;80:1–11.

[3]. Tran C, Ouk S, Clegg NJ, Chen Y, Watson PA, Arora V, et al. Development of a Second-Generation Antiandrogen for Treatment of Advanced Prostate Cancer. Science 2009;324:787–90. [PubMed: 19359544]

[4]. Evangelista L, Cuppari L, Zattoni F, Mansi L, and Bombardieri E. The future of choline PET in the era of prostate specific membrane antigen. Q J Nucl Med Mol Imaging 2019;63:19–28. [PubMed: 29383928]

[5]. Ceci F, Castellucci P, and Fanti S. Current application and future perspectives of prostate specific membrane antigen PET imaging in prostate cancer. Q J Nucl Med Mol Imaging 2019;63:7–18. [PubMed: 29521482]

[6]. Emmett L, Yin C, Crumbaker M, Hruby G, Kneebone A, Epstein R, et al. Rapid Modulation of PSMA Expression by Androgen Deprivation: Serial (68)Ga-PSMA-11 PET in Men with Hormone-Sensitive and Castrate-Resistant Prostate Cancer Commencing Androgen Blockade. J Nucl Med 2019;60:950–4. [PubMed: 30552200]

[7]. Hofman MS, Lawrentschuk N, Francis RJ, Tang C, Vela I, Thomas P, et al. Prostate-specific membrane antigen PET-CT in patients with high-risk prostate cancer before curative-intent surgery or radiotherapy (proPSMA): a prospective, randomised, multicentre study. Lancet 2020;395:1208–16. [PubMed: 32209449]

[8]. Butler L, Perone Y, Dehairs J, Lupien LE, de Laat V, Talebi A, et al. Lipids and cancer: Emerging roles in pathogenesis, diagnosis and therapeutic intervention. Adv Drug Deliv Rev 2020.

[9]. Kuemmerle NB, Rysman E, Lombardo PS, Flanagan AJ, Lipe BC, Wells WA, et al. Lipoprotein lipase links dietary fat to solid tumor cell proliferation. Mol Cancer Ther 2011;10:427–36. [PubMed: 21282354]

[10]. Swinnen JV, Brusselmans K, and Verhoeven G. Increased lipogenesis in cancer cells: new players, novel targets. Curr Opin Clin Nutr Metab Care 2006;9:358–65. [PubMed: 16778563]

[11]. Tousignant KD, Rockstroh A, Taherian Fard A, Lehman ML, Wang C, McPherson SJ, et al. Lipid Uptake Is an Androgen-Enhanced Lipid Supply Pathway Associated with Prostate Cancer Disease Progression and Bone Metastasis. Mol Cancer Res 2019;17:1166–79. [PubMed: 30808729]

[12]. Nassar ZD, Mah CY, Dehairs J, Burvenich IJ, Irani S, Centenera MM, et al. Human DECR1 is an androgen-repressed survival factor that regulates PUFA oxidation to protect prostate tumor cells from ferroptosis. Elife 2020;9:e54166. [PubMed: 32686647]

[13]. Sorvina A, Bader CA, Caporale C, Carter EA, Johnson IRD, Parkinson-Lawrence EJ, et al. Lipid profiles of prostate cancer cells. Oncotarget 2018;9:35541–52. [PubMed: 30473749]

[14]. Corsetto PA, Colombo I, Kopecka J, Rizzo AM, and Riganti C. omega-3 Long Chain Polyunsaturated Fatty Acids as Sensitizing Agents and Multidrug Resistance Revertants in Cancer Therapy. Int J Mol Sci 2017;18.

[15]. Butler LM, Centenera MM, and Swinnen JV. Androgen control of lipid metabolism in prostate cancer: novel insights and future applications. Endocr Relat Cancer 2016;23:R219–27. [PubMed: 27130044]

[16]. Watt MJ, Clark AK, Selth LA, Haynes VR, Lister N, Rebello R, et al. Suppressing fatty acid uptake has therapeutic effects in preclinical models of prostate cancer. Sci Transl Med 2019;11.

[17]. Lewis DY, Soloviev D, and Brindle KM. Imaging tumor metabolism using positron emission tomography. Cancer J 2015;21:129–36. [PubMed: 25815854]

[18]. Ackermann U, Plougastel L, Goh YW, Yeoh SD, and Scott AM. Improved synthesis of [F-18]FLETT via a fully automated vacuum distillation method for [F-18]2-fluoroethyl azide purification. Appl Radiat Isotopes 2014;94:72–6.

[19]. Wichmann CW, Goh YW, Parslow AC, Rigopoulos A, Guo N, Scott AM, et al. Synthesis and validation of [(18)F]mBPET-1, a fluorine-18 labelled mTOR inhibitor derivative based on a benzofuran backbone. EJNMMI Radiopharm Chem 2020;5:3. [PubMed: 31974638]

[20]. Pretze M, Kuchar M, Bergmann R, Steinbach J, Pietzsch J, and Mamat C. An Efficient Bioorthogonal Strategy Using CuAAC Click Chemistry for Radiofluorinations of SNEW Peptides and the Role of Copper Depletion. ChemMedChem 2013;8:935–45. [PubMed: 23559494]

[21]. Demko ZP and Sharpless KB. An intramolecular [2 + 3] cycloaddition route to fused 5-heterosubstituted tetrazoles. Org Lett 2001;3:4091–4. [PubMed: 11735592]

[22]. Centenera MM, Hickey TE, Jindal S, Ryan NK, Ravindranathan P, Mohammed H, et al. A patient-derived explant (PDE) model of hormone-dependent cancer. Mol Oncol 2018;12:1608–22. [PubMed: 30117261]

[23]. Rysman E, Brusselmans K, Scheys K, Timmermans L, Derua R, Munck S, et al. De novo lipogenesis protects cancer cells from free radicals and chemotherapeutics by promoting membrane lipid saturation. Cancer Res 2010;70:8117–26. [PubMed: 20876798]

[24]. Gubbens J, Ruijter E, de Fays LEV, Damen JMA, de Kruijff B, Slijper M, et al. Photocrosslinking and Click Chemistry Enable the Specific Detection of Proteins Interacting with Phospholipids at the Membrane Interface. Chem Biol 2009;16:3–14. [PubMed: 19171301]

[25]. Tetko IV, Gasteiger J, Todeschini R, Mauri A, Livingstone D, Ertl P, et al. Virtual computational chemistry laboratory–design and description. J Comput Aided Mol Des 2005;19:453–63. [PubMed: 16231203]

[26]. Valkó K, Bevan C, and Reynolds D. Chromatographic Hydrophobicity Index by Fast-Gradient RP-HPLC: A High-Throughput Alternative to log P/log D. Anal Chem 1997;69:2022–9. [PubMed: 21639241]

[27]. Abedi JA. High throughput HPLC method for determining log P values. European Patent Application EP1074836 2001.

[28]. Dijkstra J, van Galen M, Regts D, and Scherphof G. Uptake and processing of liposomal phospholipids by Kupffer cells in vitro. Eur J Biochem 1985;148:391–7. [PubMed: 3987696]

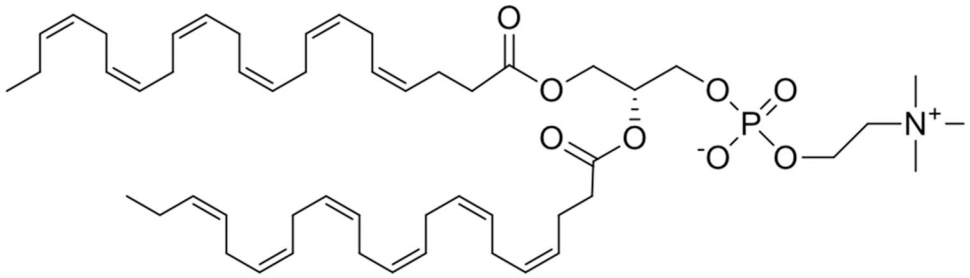

PC44:12

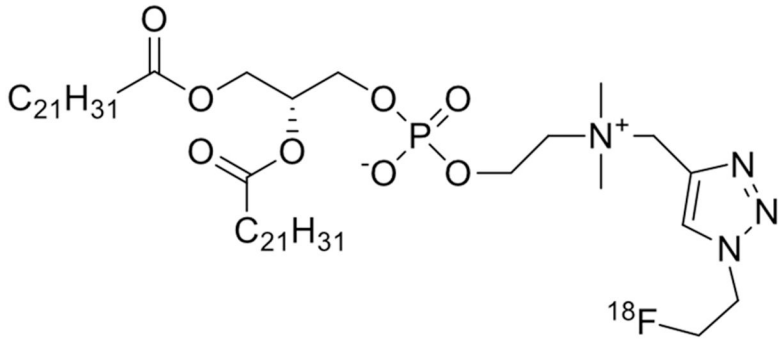

[$^{18}$F]**2**

**Fig. 1.**
Structures of PC44:12 **(1)** and [$^{18}$F]**2** **(2)**.

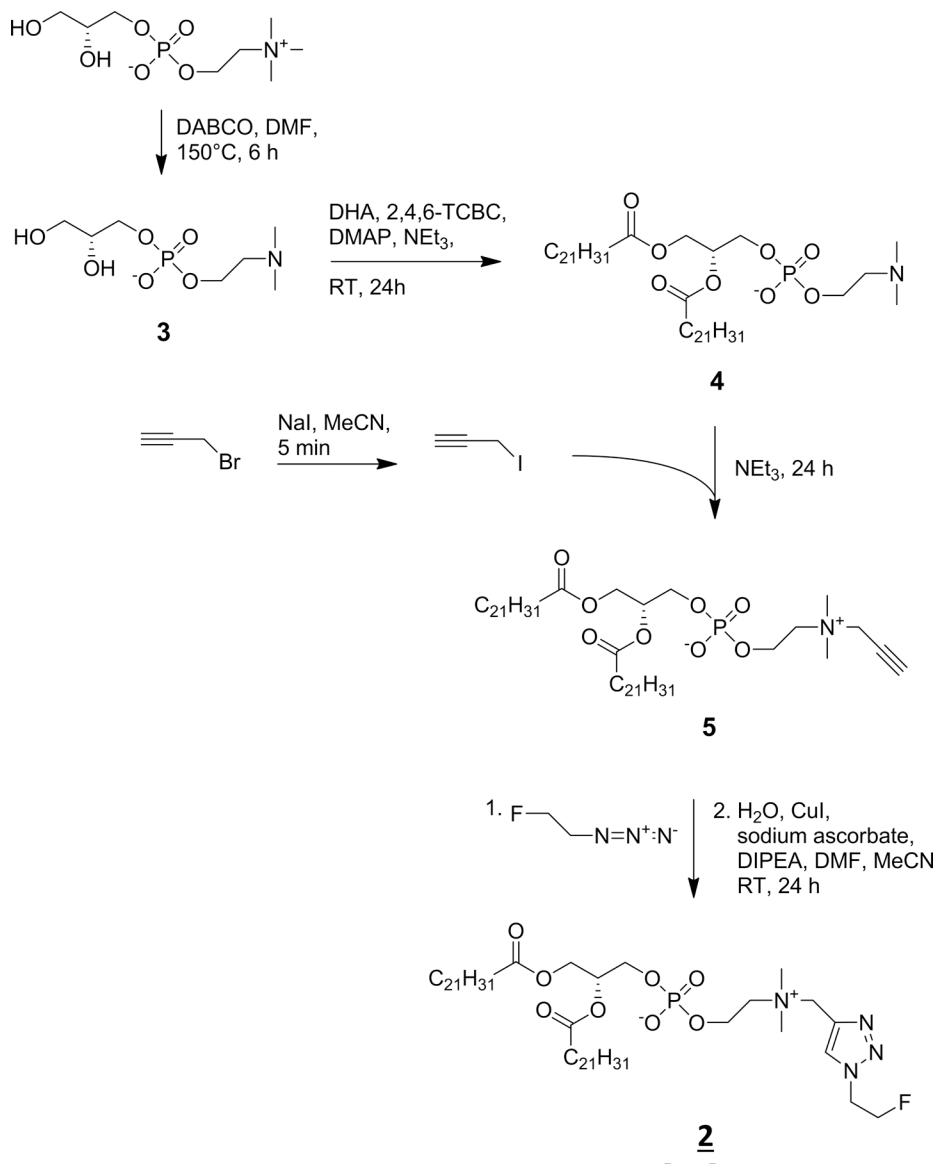


**Fig. 2.**

Reaction Scheme. Synthesis of non-radioactive standard **2**.

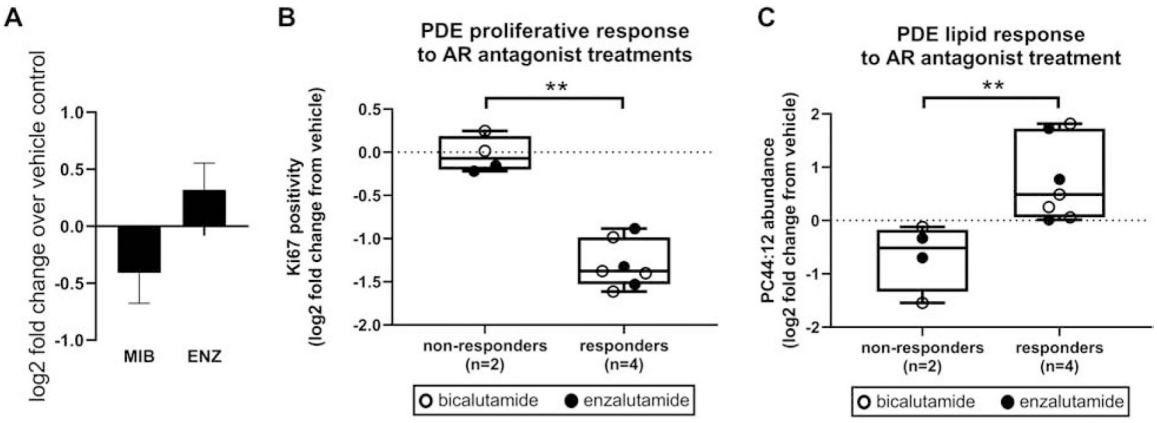


**Fig. 3.**

PC44:12, a candidate for phospholipid radiotracer development. (A) Lipidomics of LNCaP cells shows androgen regulation of phospholipid species PC44:12. MIB, miberolone; ENZ, enzalutamide. $n = 3$; bars, SD (B) Proliferative response, and (C) PC44:12 lipid response of patient-derived explants ($n = 6$) to AR antagonist (bicalutamide or enzalutamide) treatment compared to vehicle. Proliferative response, determined by immunostaining for the marker Ki67, stratified patients as non-responders ($n = 2$) or responders ($n = 4$). Box plots represent the median and interquartile range, whiskers represent the minimum and maximum values. **p<0.01; Mann-Whitney U Test.

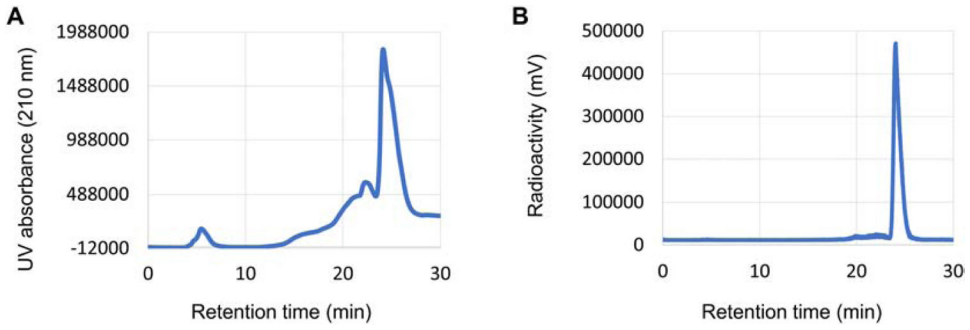


**Fig. 4.**

LC trace of 0 – 100% ethanol in water gradient over 30 minutes. (A) LC-UV of non-radioactive standard **2** with elution at 24 min, (B) Radiotrace of [$^{18}$F]**2** tracer with elution at 24 min.

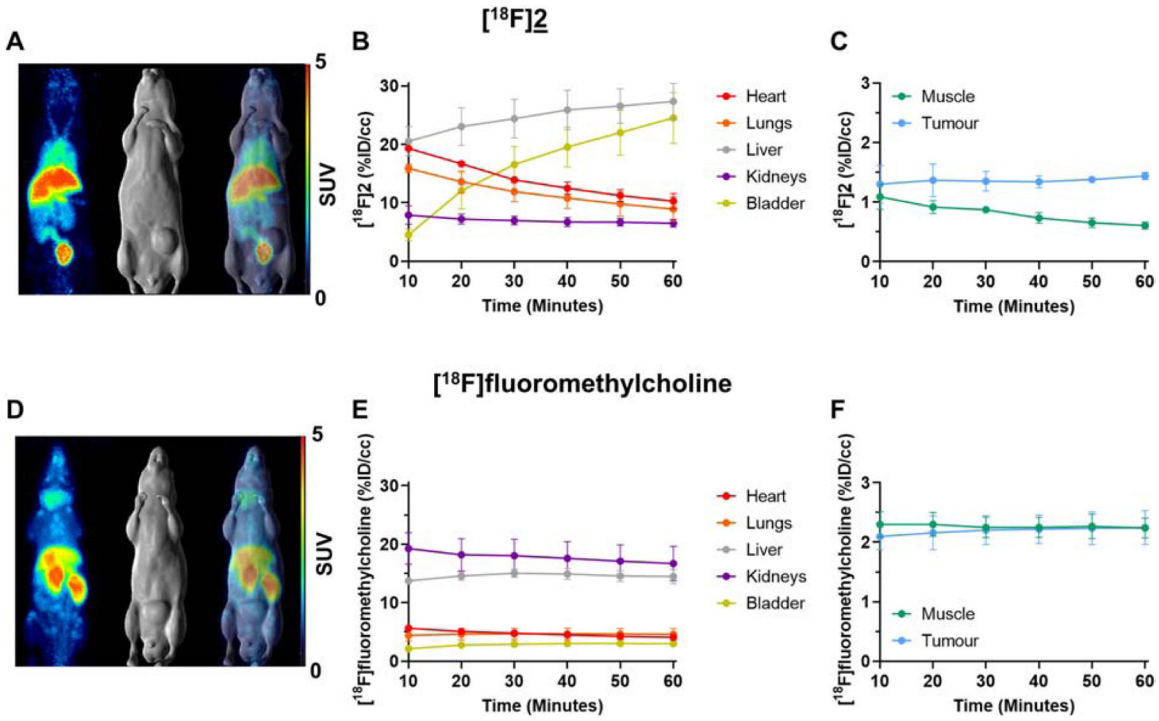


**Fig. 5.**

Dynamic PET/MRI imaging of [$^{18}$F]**2** and [$^{18}$F]fluoromethylcholine in LNCaP tumor-bearing mice. (A) Representative whole body maximum intensity projection (MIP) PET image (*left panel*), coronal MRI section (*middle panel*) and overlay PET/MRI (*right panel*) are shown of 6.6 MBq (0.178 mCi) [$^{18}$F]**2** at 60 minutes post injection. (B-C) Time activity curves of [$^{18}$F]**2** of liver, bladder, heart, lungs and kidneys (B) and muscle and tumor (C) based on VOI analysis of acquired dynamic PET images ($n$ = 3; *bars*, SD). (D) Representative whole body maximum intensity projection (MIP) PET image (*left panel*), coronal MRI section (*middle panel*) and overlay PET/MRI (*right panel*) are shown of 14.8 MBq (0.4 mCi) [$^{18}$F]fluoromethylcholine at 60 minutes post injection. (E-F) Time activity curves of [$^{18}$F]fluoromethylcholine of liver, bladder, heart, lungs and kidneys (E) and muscle and tumor (F) based on VOI analysis of acquired dynamic PET images ($n$ = 2; *bars*, SD).

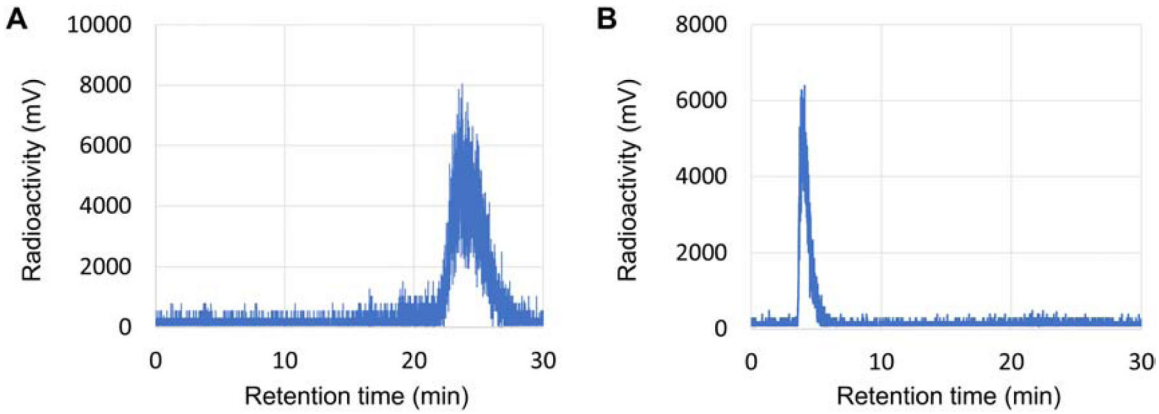


**Fig. 6.**

[$^{18}$F]**2** radiotracer and radioactive metabolites extracted from mouse liver. (A) HPLC chromatogram of organic phase with radiotracer at 24 min. (B) HPLC chromatogram of aqueous phase with polar metabolite at 4 min.

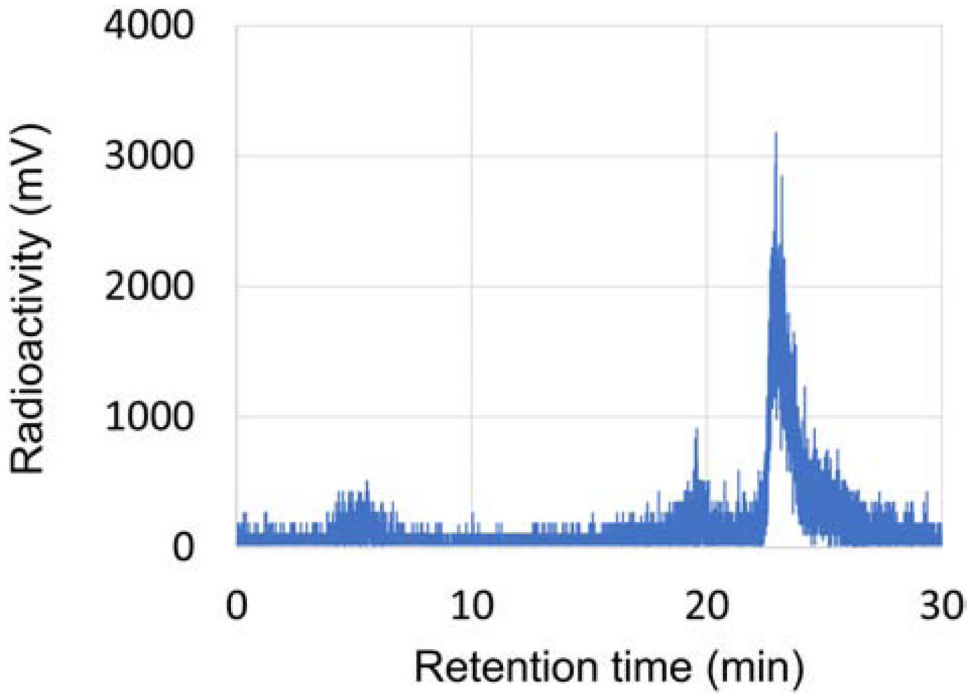


**Fig. 7.**

Mouse blood extract containing [$^{18}$F]**2** radiotracer. HPLC chromatogram at 24 min and radioactive metabolites at 5 min obtained from biodistribution study.

**Table 1**

Radiochemical yields and purities for [$^{18}$F]**2** of six synthesis runs

| Run | Yield (mCi) | Yield (%) | | Radiochemical purity (%) |
|---|---|---|---|---|
| | | Decay corrected | Not corrected | |
| 1 | 28 | 15 | 6 | >99 |
| 2 | 21 | 9 | 5 | >99 |
| 3 | 34 | 17 | 6 | >99 |
| 4 | 34 | 21 | 12 | 95 |
| 5 | 30 | 11 | 6 | 95 |
| 6 | 95 | 34 | 19 | 95 |

## Table 2

Estimated log *P* values and retention times of reference compounds and non-radioactive standard **2**

| Compound | Retention time | log *P* | |
|---|---|---|---|
| | (min) | ALOGPS | ChemAxon |
| Choline | 4.25 | −3.59 | −4.66 |
| Caffeine | 17.0 | −0.24 | −0.55 |
| Ibuprofen | 26.4 | 3.50 | 3.84 |
| Trans-Retinoic acid | 31.2 | 5.66 | 5.01 |
| Cholecalciferol | 45.0 | 7.98 | 7.13 |
| α-Tocopherol | 51.5 | 8.84 | 10.51 |
| **2** | **41.0** | **6.9** | **7.2** |

**Table 3**

Tissue biodistribution of [$^{18}$F]**2** lipid in LNCaP tumor-bearing NOD SCID Gamma mice at 50 minutes post injection

| Tissue | Uptake (%ID/g)* |
|---|---|
| Blood | 6.1 ± 3.0 |
| Brain | 0.5 ± 0.3 |
| Heart | 2.4 ± 1.2 |
| Lung | 3.5 ± 1.1 |
| Stomach | 1.4 ± 0.8 |
| Spleen | 10.9 ± 9.1 |
| Liver | 41.1 ± 9.2 |
| Kidney | 4.8 ± 1.2 |
| Small Intestines | 6.0 ± 2.7 |
| Large Intestines | 1.2 ± 0.3 |
| Muscle | 0.3 ± 0.1 |
| Bone | 0.8 ± 0.3 |
| Skin | 0.4 ± 0.1 |
| Tumor | 0.8 ± 0.3 |

*data presented as mean ± SD, $n = 3$